TDK Thesis

Giuseppe Mark Marcello
2018

Quantitative electron microscopic analysis of the brain in the CNTNAP2 mouse model of autism

author: Giuseppe Mark Marcello
supervisor: Bence Rácz, PhD, associate professor
University of Veterinary Medicine Budapest,
Department of Anatomy and Histology

2018

Table of Contents

Abbreviations in alphabetical order

ASD autism spectrum disorder

AVP arginin vasopressin

CD-FES cortical dysplasia-focal epilepsy syndrome

CNTNAP2 contactin associated protein-like 2 (protein)

Cntap2 contactin associated protein-like 2 (gene)

CSF cerebral spinal fluid

DAB 3,3'-diaminobenzidine

dH_2O distilled water

E/I excitatory/inhibitory

GABA γ-aminobutyric acid

IHC immunohistochemistry

mag magnification

mPFC medial pre-frontal cortex

MSB multi-synaptic bouton

OXT oxytocin

PB phosphate buffer

PPE personal protective equipment

pPSD perforated postsynaptic density

PSD post synaptic density

PVH paraventricular hypothalamic nucleus (= PVN referred to as: paraventricular nucleus)

qEM quantitative electron microscopy

q in 7q35 (q) or long arm of chromosome 7 location 35

RMP resting membrane potential

Introduction

Prevalence and relevance of autism spectrum disorder

Brains can be divided between neurotypical and autistic. Autism spectrum disorder (ASD) includes low functioning individuals with limited capability to function alone in society as well as most probably some of the most innovative thinkers of our world (Grandin, 2010). According to the Developmental Disabilities Monitoring Network of the CDC, as of April 2018, 1 in every 56 children born are identified with ASD with the average prevalence of autism estimated between 1-2 % globally (Autism Spectrum Disorder (ASD), 2018). Working towards understanding the autistic brain is not only clinically relevant for alleviating the often-debilitating social difficulties of ASD's manifestations as a neuropsychiatric disease but for understanding the human brain in its individually colorful complexity.

Autism has a remarkably high phenotypic heterogeneity (Lazaro, 2017). To date ASD is defined by a broad set of social behaviors: impairments of social communication, restricted interests, and repetitive behaviors (Weiss et al., 2016). This wide clinical definition includes: autistic disorder, Asperger's disorder, childhood disintegrative disorder, and pervasive developmental disorder not otherwise specified (Weiss et al., 2016). Neurobiological mechanisms of development and differential mature functionality underlie the clinically complex presentation of autism (Foxe et al., 2018). There is ample evidence, such as malfunction of cortical lamination, which suggests a neurodevelopmental basis for ASD (Strauss et al., 2006). There are two main issues in researching the neurobiology of ASD: 1. linking cellular processes to genetic background, and 2. processing ample brain tissue. As an approach to the first issue, syndromic forms of autism with known genetic basis are used to precisely simplify ASD in order to form more targeted questions. Mouse models are one answer to the second issue as there is simply not enough human ASD brain to study. Combining the two approaches: mouse models of syndromic forms of ASD allow for the dissection of the neurodevelopmental and mechanistic underpinnings of autism by engineered gene knock outs (KOs). We study a contactin associated protein-like 2 (CNTNAP2) KO mouse model of a syndromic form of ASD: *cortical dysplasia-focal epilepsy syndrome* (CDFES).

CNTNAP2 KO mouse-model of a syndromic form of autism: CDFES

CDFES is described in a group of *'Old Order Amish children'* who presented with focal seizures in early childhood which deteriorated their learning ability and social behavior (Strauss et al., 2006). CDFES has autosomal recessive inheritance (Strauss et al., 2006). Three patients with CDFES underwent surgery to control their seizures; the excised tissues were immunohistochemically (IHC) processed (Strauss et al., 2006). Cortical developmental pathology is supported by findings of blurring of the gray matter and white matter junction and numerous ectopic neurons in subcortical white matter (Strauss et al., 2006). Additionally, neocortical cells which were described to have a spherical rather than a pyramidal profile, abnormal dendrite structure and neurofilament tangles (Strauss et al., 2006). Primary findings in CDFES are noteworthy as findings in CNTNAP2 ASD mouse model are compared to this syndromic form of ASD. As such, it must be considered that in humans this genetic lesion is a nonsense mutation while in mice it is a null mutation (Strauss et al. 2006). Studies in human as well as mouse models present excitatory/inhibitory (E/I) imbalance toward hyperexcitability which may contribute to the comorbidity of autism and epilepsy. In post-mortem samples of human ASD patients neuropathological findings indicate a reduction of minicolumns, neocortical structures of excitatory pyramidal neurons surrounded by GABAergic inhibitory neurons (Bozzi et al., 2017). Also, EEG data in people with ASD points to increased interictal spikes indicating epileptiform activity (Bozzi et al., 2017). These findings in human ASD and particularly in CDFE provide the backdrop for the investigation of our CNTNAP2 mouse model E/I balance.

The genetic background of CDFES in humans is a truncating mutation which results in the premature termination of translation before the putative transmembrane domain of the protein (Strauss et al., 2006). CNTNAP2 is the alpha isoform of Caspr2, the largest coded protein of the gene Cntnap2. The cytogenic location of the CNTNAP2 associated genetic lesion is on chromosome 7 at 7q35-7q36 (Kniffin, 2017). Of mice, constitutive knock-out (KO) mice were engineered with a loss of function mutation in CNTNAP2 (Lazaro, 2017). A congenic, targeted (null/knock out) mutation produced in the start codon containing exon 1 produces the mouse marketed as B6.129(Cg)-*Cntnap2*^{tm1Pele}/J (B6.129(Cg)-Cntnap2tm1Pele/J., 2018).

CNTNAP2 is a member of the neurexin protein superfamily, and it is widely expressed in the brain (**Figure 1.)** (Poliak et al., 1999). CNTNAP2 mediates cell-cell interactions in the nervous system (Poliak et al., 1999). Its described functions include clustering potassium

channels in the juxtaparanode, mediating neuron-glia interactions, neuronal migration, and as transynaptic structural scaffolding (Poliak et al., 2003, Rodenas-Cuadrado et al., 2014).

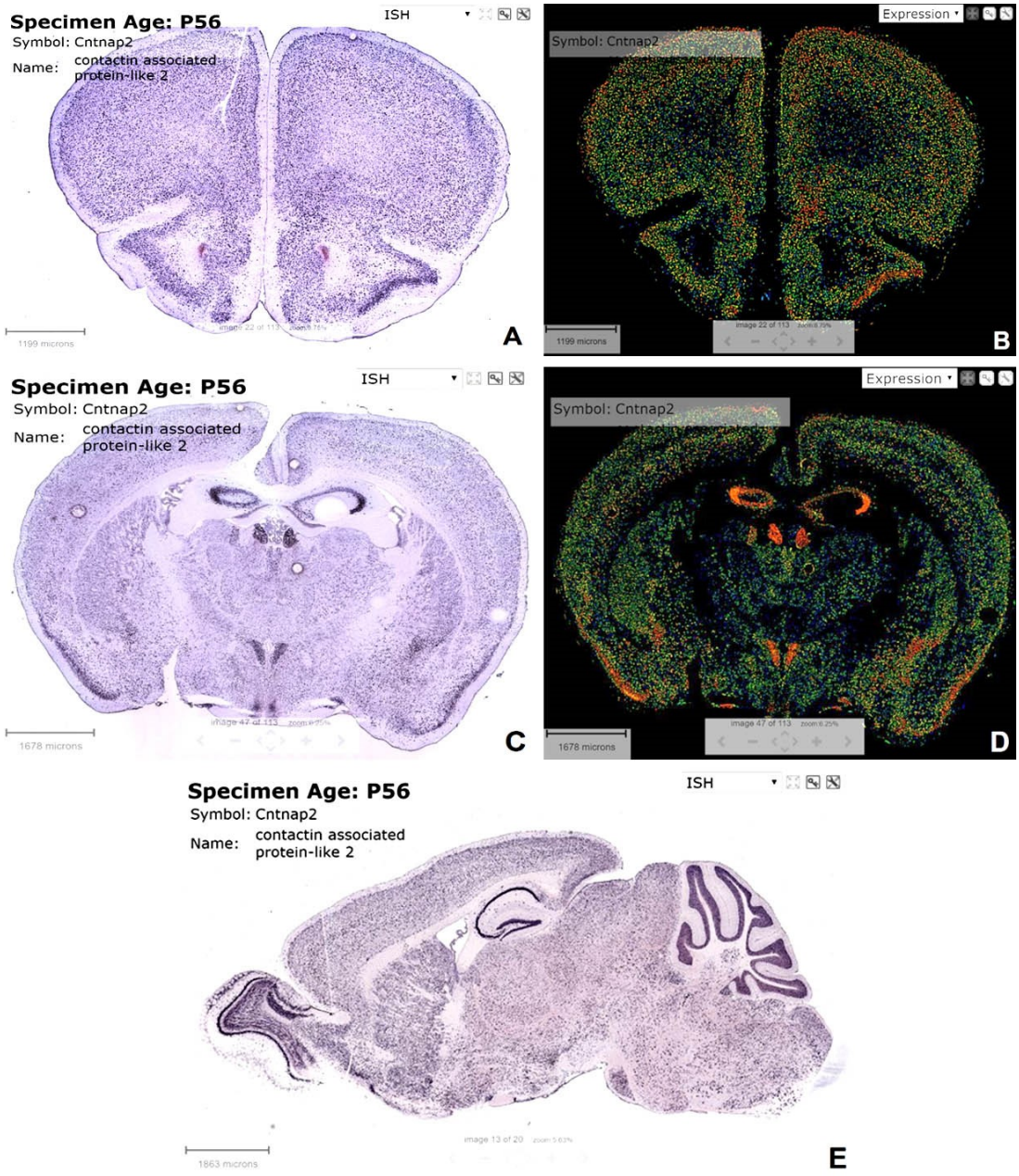

Figure 1. CNTNAP2 expression from Allen brain ISH Reference Atlas. A. Coronal section showing in situ hybridization (ISH) of Cntnap2 showing IHC expression of CNTNAP2 coding RNA in mPFC, note darker purple staining (for schematic of mPFC see **Fig. 2 A**). **B.** Coronal section in mPFC plane showing ISH fluorescent expression of Cntnap2, note: warmer colors (red-oranges) for stronger ISH signal indicating more protein expression. **C.** Coronal section showing ISH of Cntnap2 showing IHC expression of CNTNAP2 coding RNA in PVH, note: butterfly-like dark purple staining tissue ventrally (for schematic of PVH see **Fig. 3 A**). **D.** Coronal section in section plane of PVH showing ISH signal of Cntnap2 expression. **E.** Sagittal section showing IHC staining of ISH showing brain-wide expression of Cntnap2. (*Allen brain atlas ISH data, mouse.brain-map.org*)

CNTNAP2, as a neurexin, is a polymorphic synaptic receptor as well as a transsynaptic structural element (Sudhof, 2008). As a part of the exciting field of transynaptic molecular pathways, CNTNAP2 forms a complex with neurolignins and interacts in a variety of ways with partner on the opposite side of the synaptic cleft (Sudhof, 2008). It is well established that CNTNAP2 functions as an organizer of axonal microdomains in myelinated nerves but its role in neuronal development, migration, and cortical network function are lacking (Anderson et al., 2012). CNTNAP2 is tied to assembly of neural circuits and may play a role in controlling the growth of dendritic arbors and spines before myelination (Anderson et al., 2012).

The mPFC and PVH in human ASD and CNTNAP2 KO ASD mouse-model brain

Our collaborators in Peyman Golshani's lab in UCLA investigated layer 2/3 (L 2/3) of the prelimbic medial prefrontal cortex (mPFC) of the CNTNAP2 KO mouse model of autism (**Figure 2.**). By electrophysiological measurement they found delayed phase-firing and reduced phase-locking of inhibitory and excitatory neurons (Lazaro et al., 2018). Investigating CNTNAP2's role in dendritic arborization, our collaborators found anatomical differences in dendrite morphology and spine density at light microscopic magnification (mag), particularly: decreased spine density in pyramidal neurons (Lazaro, 2017). Lazaro et al. approached our lab to investigate these network E/I imbalances and dendrite morphological results at electron microscopic (EM) mag. We performed quantitative electron microscopy (qEM) on L2/3 of the prelimbic mPFC investigating dendrite spine density, E/I synapse density, and synaptic ultrastructural measurements.

In our qEM investigation of the mPFC of the CNTNAP2 KO ASD mouse model we measured synaptic ultrastructure. We took the number of multisynaptic boutons (MSBs), axon terminals which transmit to more than one dendritic spine, to indicate synapses which were presynaptically robust and strongly functioning; similarly, perforated post synaptic densities (PSDs) were taken as a mark of powerful postsynaptic strength/excitability (Sorra and Harris, 1993; Bourne and Harris, 2008). In addition to these measures of excitatory synaptic strength, over-all spine number was measured. With a postsynaptic focus, parameters of synaptic ultrastructure were measured. Spine area and circularity were measured. Spine profile morphology is directly relatable to its conductance, excitability and efficacy of transmission (Harris, 1999). We also quantified total number of symmetrical (putative inhibitory) synapses to compare with electrophysiological recordings of network E/I.

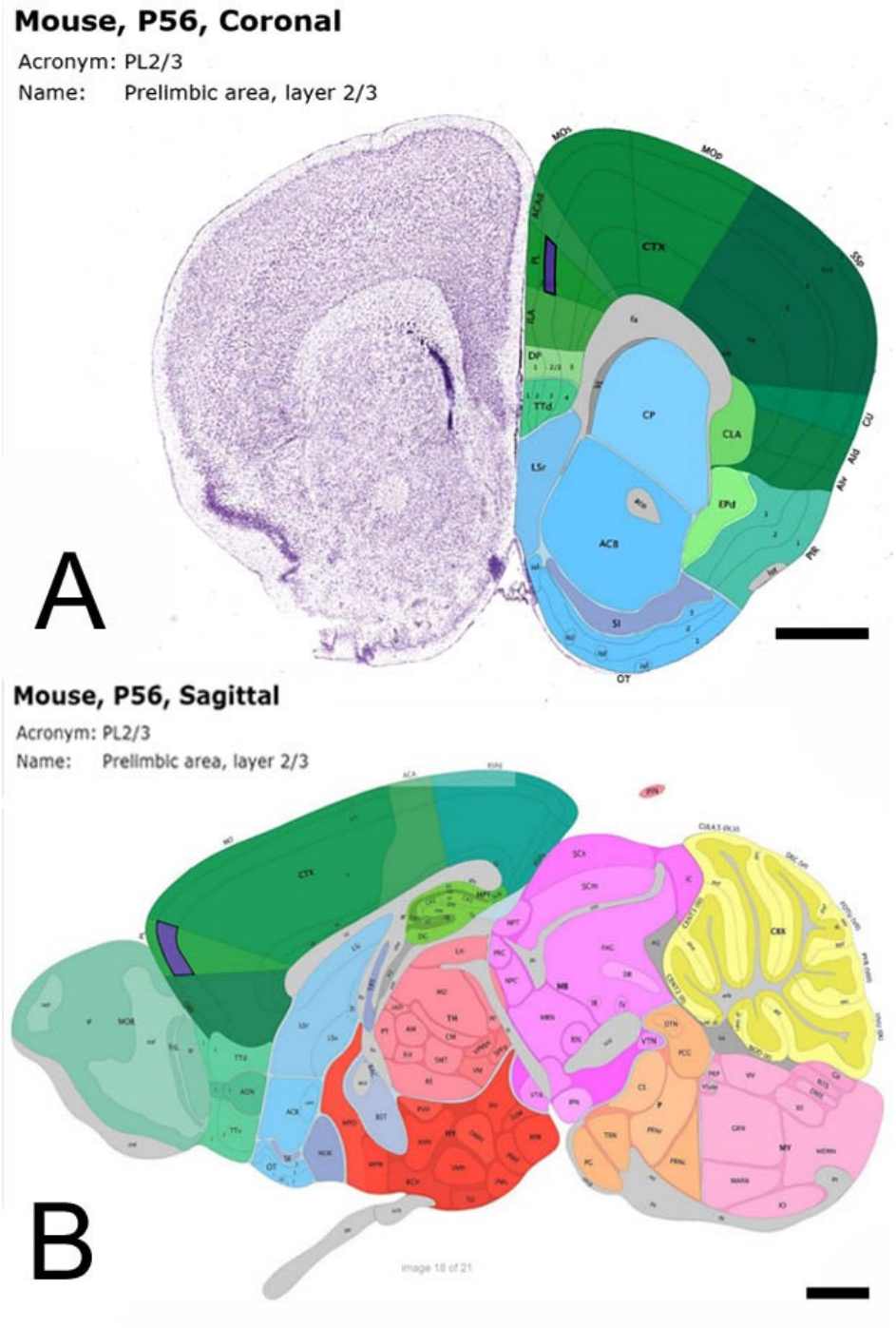

Figure 2. prelimbic mPFC Layer 2/3. A. Coronal section from reference atlas at section plane of mPFC. Dark purple area on schematic shows Layer 2/3. Nissl staining on other side shows gross morphology for orientation. **B.** Sagittal section from reference atlas indicating mPFC L 2/3 area (dark purple) for orientation with regard to intact brain. (source: Allen mouse brain atlas reference atlas, mouse.brain-map.org/static/atlas) Scale bar: 1mm

Naturally following the conclusion of our analysis, Choe et al. (also at the UCLA Golshani lab) approached us with an investigation of a different brain region in the CNTNAP2 KO ASD mouse-model related to the central oxytocin (OXT) system: the paraventricular hypothalamic nucleus (PVH, **Figure 3.**). We investigated the glial endfoot coverage of

oxytocinergic magnocellular neuronal somata in the magnocellular division of the PVH. Glial coverage raises possibilities of network dynamic change and a possible avenue for CNTNAP2 mechanistically through neuronal-glial interaction. In the magnocellular division of the PVH, oxytocinergic magnocellular neurons are adjacent to vasopressinergic magnocellular neurons. OXT and arginine-vasopressin (AVP) are observed to have opposite effects in the brain (de Wied et al., 1993). We assessed general glial coverage in a native qEM analysis. Following, we used immunohistochemical (IHC) methods to specifically label OXT neurons. We analyzed these OXT antibody marked neurons with qEM. Immune labeling and ultrastructural analysis was performed after Theodosis et al. 1986. Our investigation of the magnocellular neurons in the PVH built on this study's glial endfoot coverage analysis and neuronal apposition analysis in the supraoptic nucleus of the hypothalamus (the only other place in the brain OXT and AVP neurons exist) (Theodosis et al., 1986).

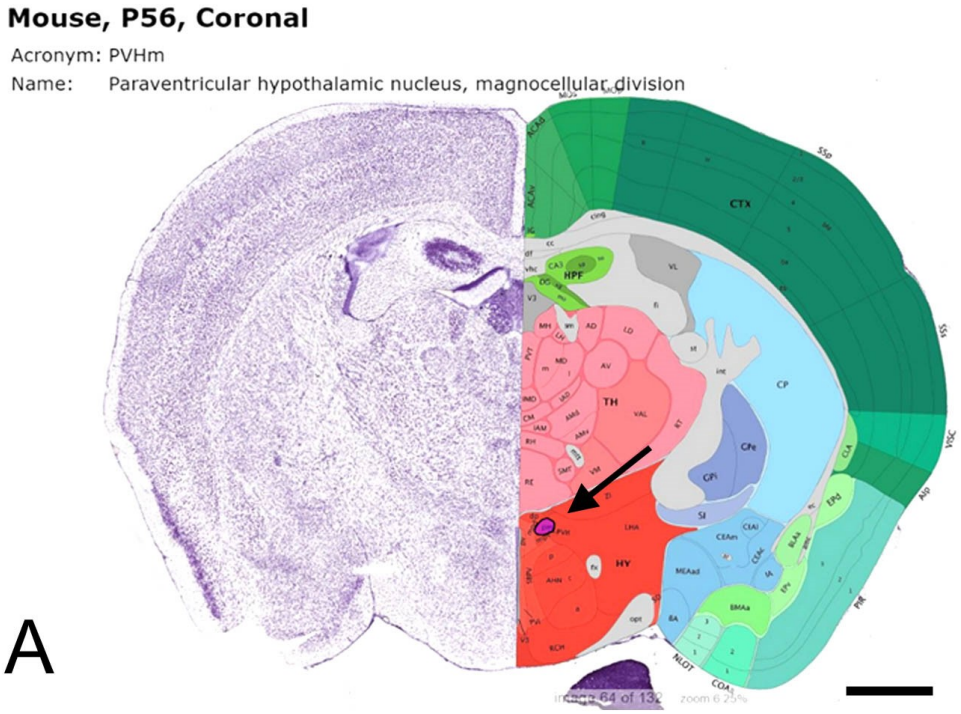

Figure 3. PVH magnocellular division and oxytocin cells. A. Coronal section in reference atlas at section plane of PVH, indicating PVH magnocellular division in dark purple (arrow) in schematic with Nissl staining on other side. (source: Allen mouse brain atlas reference atlas, mouse.brain-map.org/static/atlas) Scale bar: 1 mm

The social behavioral abnormalities of CNTNAP2 KO mouse model were investigated by Peñagarikano et al. 2011; marked decrease in pup to mother ultrasonic vocalizations after separation, decrease in time of juvenile play and a significant increase in grooming and digging activity are described. CNTNAP2 KO mice develop spontaneous seizures ~6 months of age

before which they exhibit a range of behavioral differences as compared to WT (Vernes et al., 2014). This early onset of seizures is similar to the early onset seizures described in CDFES (Strauss, 2006). Interestingly, Peñagarikano et al. 2015 shows a rescue of social behavior in CNTNAP2 KO mouse, as significant increase in performance in reciprocal social interaction test, by intraperitoneal injection and intranasal spray of oxytocin. Exploring mechanistic aspects of the OXT system in ASD is of particular interest due to recent clinical trials of intranasal OXT application as a pharmacological intervention to rescue debilitating social behavioral abnormalities (Parker 2017).

With only a general social behavioral clinical characterization, any consistent neurobiological mechanism of ASD is lacking. As Foxe et al. points out in the March 2018 special edition of the European Journal of Neuroscience, the field cannot say with confidence that there are consistent structural anatomical findings in ASD thus the search for mechanisms is ungrounded. The power of qEM analysis is tying together structure and function. With our contribution to work done in the mPFC and the PVH by our collaborators we look to give some morphological basis to various modes of CNTNAP2 action.

Aims

Using the analytic power of qEM on the CNTNAP2 KO mouse model of a syndromic form of autism, we aim to illuminate changes ultrastructural parameters in two brain regions linked to change in function of the human autistic brain. Two sets of parameters are analyzed with two sets of goals.

1. *In layer 2/3 of the pre-limbic mPFC*: density of E/I synapses, numbers of spines, and synaptic ultrastructural parameters were measured. The aim was to quantify structural differences implicating changes of synaptic functionality.
2. *In the magnocellular division of the PVH*: glial endfoot coverage of magnocellular neurons was quantified. The aim was to explore a morphologically observable mechanistic change in the function of the central oxytocin system.

Methods

Brains to ultrathin sections

Brains were received as ice cooled packages mailed from collaborators in UCLA. Intact brains of 3 KO and 3 WT mice were suspended in 2% paraformaldehyde and 2% glutaraldehyde fixative. Processing from intact brains to ultrathin sections was done according to Marcello et al. (2018). Both WT and KO animal brains were dissected by a razor blade under stereomicroscope to coronal wedges for general area containing each respective brain region. A wedge was cut rostrally containing the mPFC. The remaining brain was dissected to a wedge containing the PVH. Dissection under stereomicroscope was aided by Allen Brain Reference Atlas, see **Figure 2.**, and **Figure 3.**

Brain wedges were individually mounted on a vibratome plate using a small drop (~50 µl) of superglue only. The chamber of the vibratome was filled with 0.1 M PB. With vibratome sectioning 60 µm thick free-floating sections were obtained. Due to the robust fixation of the material (in high concentration of glutaraldehyde) a higher speed and lower frequency of vibration was used. Free-floating sections containing the area of interest were collected into glass vials containing 0.1 M PB using a round bristle paint brush. At this point immunohistochemistry was performed on free-floating sections, see section OXT IHC. Without immune reaction the samples were processed in native contrast for qEM analysis. All sections were embedded in resin as described below.

Free-floating sections were incubated for 2 x 5 min in 0.1 M PB (pH 7.4). Sections were then incubated for 1 h in a solution of 1% osmium tetroxide and 0.1 M PB (pH 7.4); this incubation step was performed under a hood with appropriate PPE. The sections were again incubated for 2 x 5 min in 0.1 M PB (pH 7.4), this step is a stopping point at which the sections may be stored in the refrigerator overnight. The sections were then incubated in an ethanol series for dehydration: 5 min in 30% ethanol followed by 5 min in 50%, 70%, 80%, 95% ethanol and 2 x 5 min in 100% ethanol. Free-floating sections were then incubated for 5 min in 1:1 100% ethanol/propylene oxide followed by incubation for 2 x 5 min in 100% propylene oxide. Sections were then incubated for 30min in 1:1 propylene oxide/resin (durcupan resin, hereby referred to simply as ‘resin’) followed by 1 hr in resin. At the second incubation step, in pure resin, the sample was stored in the refrigerator overnight.

The sections were waferized through the following procedure. A sandwich of 5 layers was made:

1. Glass slide;
2. A rectangular ACLAR film, bigger than the glass slide by 1-2 mm in each direction (ACLAR film cut from A4-sized film);
3. The osmicated, resin infiltrated sections were directly transferred onto the ACLAR film using a flat wood cuticle stick with an extra bit of resin; sections were arranged neatly on film;
4. Sections covered with another ACLAR film of the same size as the one beneath the tissue samples; bubble formation was avoided;
5. Name/ID of samples were scratched onto top layer glass slide with a diamond point glass engraving pen;

note: each layer of the sandwich should be staggered and unevenly stacked to facilitate the separation of the sandwich after heat curing of the resin.

The 5-layer sandwiches were put into a thermostat at 60 °C for 38-48 h to polymerize the resin. After heat curing the resin so, the upper glass slide and the upper ACLAR film was removed leaving layers 1-3 of the sandwich. The cured resin embedded sections were labeled with name/ID by permanent marker.

Under stereomicroscope a ~1-2mm^2 square or trapezoid of approximate corresponding size was cut from the resin embedded sections by a No. 11 scalpel blade, see **Figure 8. A-B**. For the precise brain region, the Allen brain reference atlas was consulted (**Figure 2. and 3.**). Layer 2/3 of the pre-limbic mPFC was identified and cut; magnocellular division of PVH was cut. Compare Nissl staining of reference atlas in **Figure 1.-3.** to **Figure 8. A.**, resin offers notable less morphological reference points in native contrast. The respective square/trapezoid of brain section was transferring with scalpel blade and mounted on a resin block with superglue under stereomicroscope.

Resin blocks with mounted sections were sectioned under a ultramicrotome; 50-70 nm thin ultrathin sections may be seen in **Figure 4.** Sections were mounted on 300 mesh copper grids. Grids were collected in a grid box. Ultrathin sections on grids were contrasted using Leica's Ultrathin II lead citrate solution by making ~50 µl droplets on a Petri dish covered by Parafilm incubating the grids on these droplets for 1 min. Grids were handled using reverse closing forceps; perfect loop was used to facilitate handling of grids. After incubation on the

droplets traces of lead contrast solution were eliminated by quickly (and gently) dipping the grids into three consecutive dH_2O filled glass vials. For each animal, the first two sets of grids with corresponding sections were contrasted and labeled accordingly on the gird box.

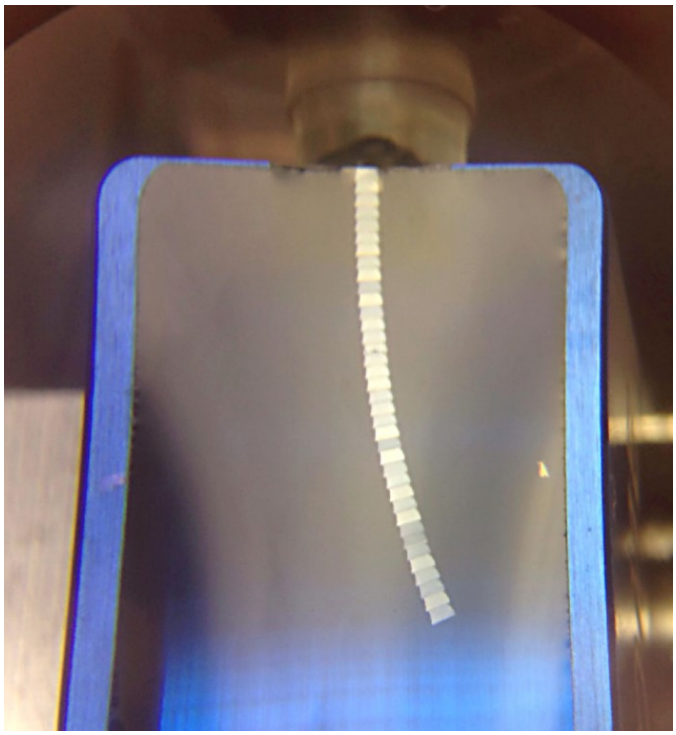

Figure 4. Ribbon of ultrathin (70-50nm) sections as seen under ultramicrotome. (image credit: Tünde Magyar)

OXT IHC

Immunohistochemistry (IHC) was used to specifically mark oxytocinergic magnocellular neurons of the magnocellular division of the PVH. Free floating sections ~60µm thick, after sectioning with vibratome, were immersed in 15-30% sucrose solution for at least 12hours, until the sections sunk to the bottom of the solution. The sugar immersed samples were cooled in liquid nitrogen to carefully loosen and perforate the cell membranes of the brain tissue for better penetration of the OXT antibody. Liquid nitrogen was poured into an appropriate container e.g. small dewar cylinder. Sucrose immersed free-floating sections were poured into a small aluminum bowl. The aluminum bowl containing the sucrose immersed free-floating sections were placed on top of the liquid nitrogen with long metal hooked forceps. The bowl was rapidly lifted after ~4 seconds floating on the liquid nitrogen; the sections were lifted out before they made a cracking sound. The notable white color of the sections confirmed

successful reaction. Sections were transferred to 0.1 M PB and washed 2 x 5 min in 0.1 M PB (pH 7.4) before IHC was started.

Pre-embedding IHC was performed according to Racz and Weinberg 2006. Monoclonal oxytocin antibody (PS series 38, highly specific against mammalian neurophysin) was used as primer at 1/100 concentration. The IHC reaction was rendered more powerfully electrondense by using 3,3'-diaminobenzidine (DAB). Reactivity of OXT antibody and appropriate concentration were determined according to Ben-Barak et al. 1985.

Image acquisition

Samples were examined by transmission electron microscope according to specific ultrastructural parameters of studying PFC or PVH. Sections of layer 2/3 prelimbic mPFC were processed by native contrast. The neuropil of the mPFC sections were photographed at 20,000X magnification (mag). These relatively low mag images suit counting of dendritic spines and synapses as well as measuring synaptic ultrastructural parameters (e.g. PSD length, spine area, spine circularity, number of MSBs and pPSDs). Viewing sections of the magnocellular division of the PVH however demanded a different set of magnifications due to the different ultrastructural parameters measured. We took electron micrographs of 8 neurons for each animal (3 KO, 3 WT) looking to measure glial coverage ratio of magnocellular neurons of the PVH. Whole neurons with the surrounding touching neuropil was included in one image (mag ranging from 7,000X-15,000X depending on size of neuron in section plane). This overview image was used to measure neuronal profile perimeter. Following this, a series of 2-5 higher mag images (ranging from 10,000X - 20,000X magnification) were taken of the surrounding touching neuropil. These series of photos were used to measure glial endfeet touching the neuronal membrane. For native contrast, electron micrographs were taken of either magnocellular neurons were either AVP or OXT. For OXT immune labeled samples, OXT neurons were identified based on specific DAB staining of intracellular OXT reactive puncta, see **Figure 8. E**. Image acquisition in EM is a marked transition in the experiment from analog to digital data. EM photos were taken and quantified blindly to eliminate bias.

EM to qEM: measuring ultrastructure on electron micrographs

All ultrastructural measurements of electron micrographs were performed in Image J v1.51j8, a software engine provided by NIH. In mPFC: dendritic spine number, asymmetrical (putative excitatory) synapse number, and symmetrical (putative inhibitory) number was measured. Additionally, numbers of MSBs and pPSDs were quantified. Synaptic ultrastructural parameters of spine profile area and circularity as well as PSD length were measured, see **Figure 5.**

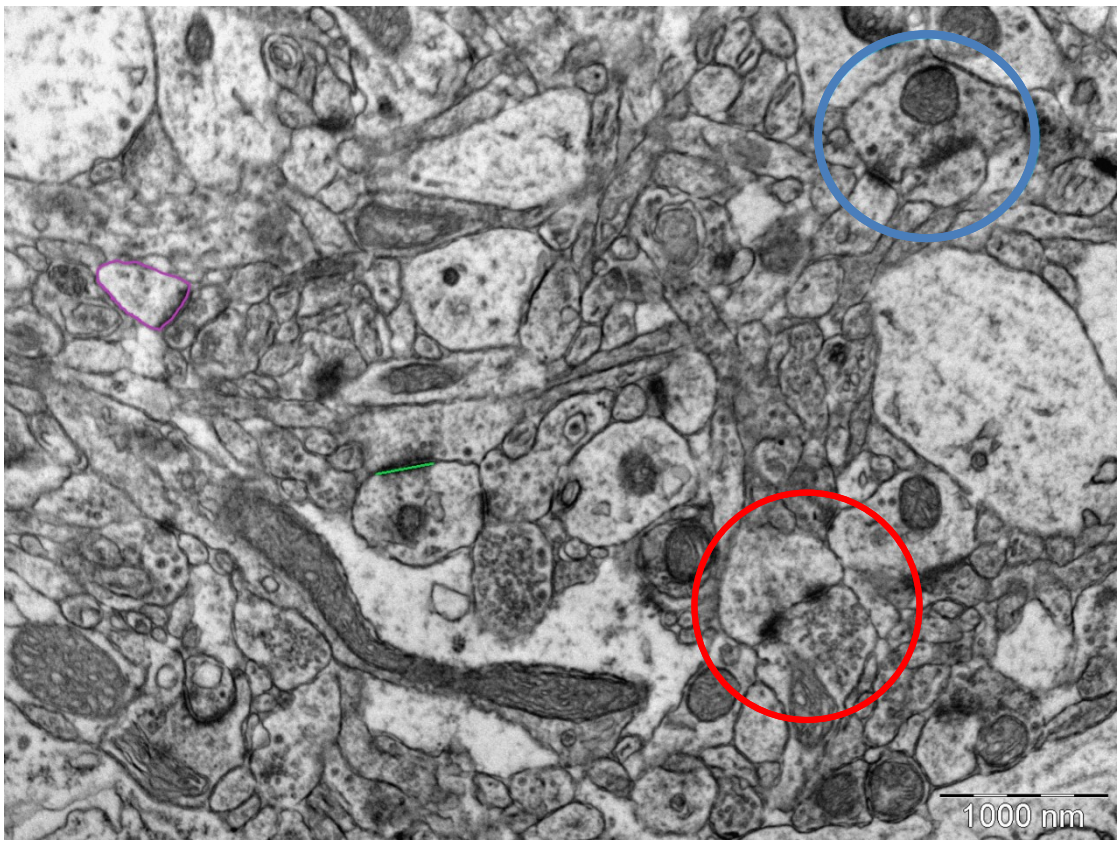

Figure 5. Ultrastructural measurements from electron micrograph of mPFC neuropil (mouse #3160). Blue circle indicates a multi-synaptic bouton (MSB) with a mitochondria in the terminal bouton. Red circle illustrates a perforated post synaptic density (pPSD). Green line indicates PSD length measurement. Pink outline represents perimeter measurement from which spine area and circularity are calculated. (20,000 X mag)

In the PVH: for each neuron the perimeter of the cell body of the neuronal profile was traced from a low mag image (7,000X-15,000X), see **Fig. 6 A**. Aided by a series of higher mag images (10,000X - 20,000X), glial endfoot coverage was measured, see **Fig. 6 B**. Glia endfeet were identified solely based on their light appearance; cytoskeletal structure and free-floating cytoplasmic proteins of glia impart a low electron density to their profile in EM (Harris and

Weinberg 2012). Glial coverage ratio was calculated by dividing diving total glial coverage by perikaryon profile perimeter.

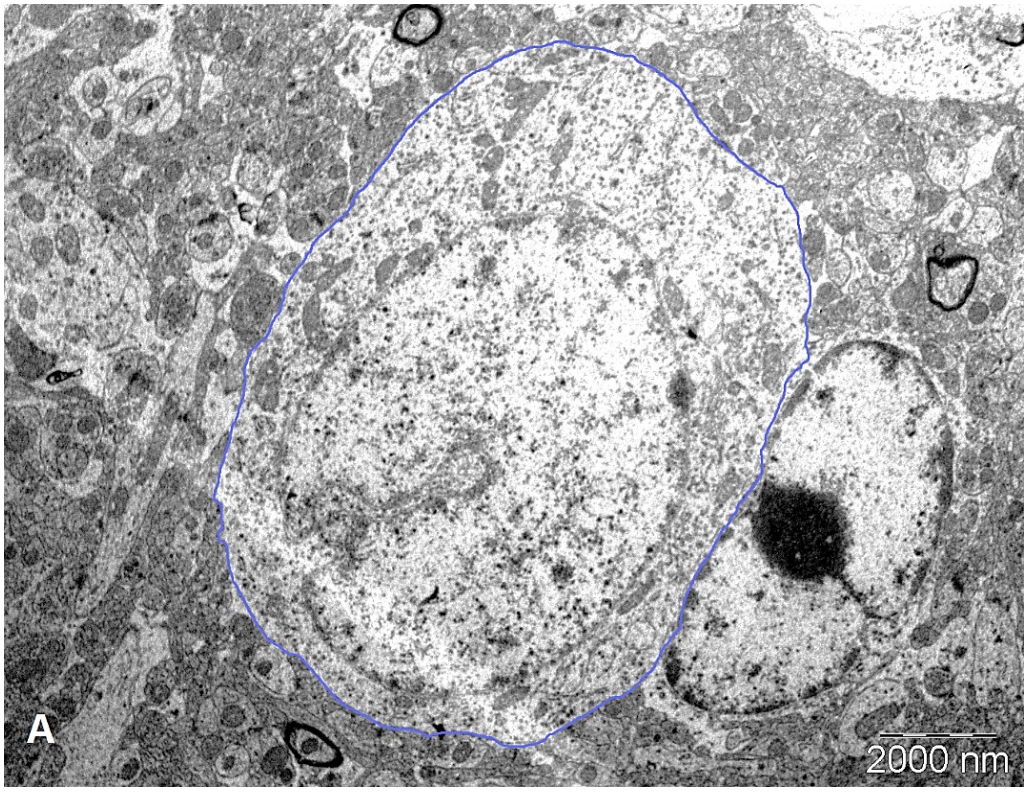

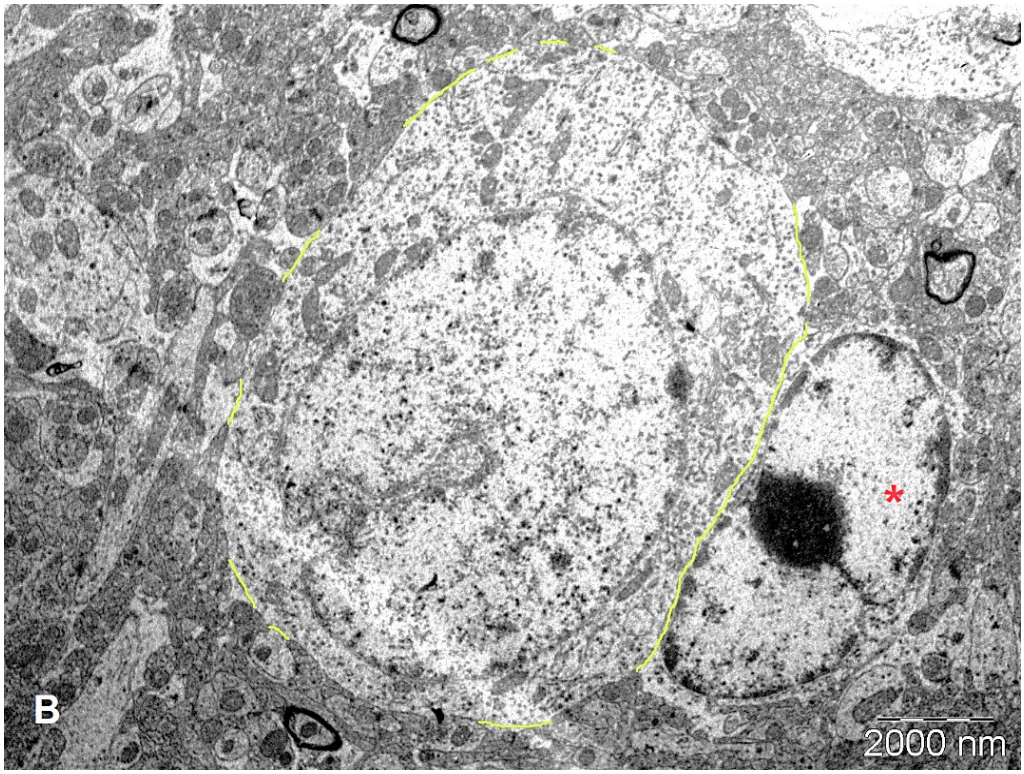

Figure 6. Analyzing glial endfoot: neuron coverage from electron micrograph in PVH (mouse 3170). **A.** perimeter of OXT/AVP magnocellular neuronal profile indicated with blue freehand line. **B.** glial endfoot coverage of neuronal profile indicated with light green segmented free hand lines. Individual endfeet measurements are schematically shown on low mag electron micrograph for clarity but a series of 2-5 higher mag electron micrographs were used for measurement. Red asterisk (*) indicates astroglia profile. (7,500 X mag)

Statistical analysis

The data were compiled using Excel (Microsoft) and Kaleidagraph (Synergy Software) software. For mPFC, effects of the loss of CNTNAP2 gene were determined by comparing difference of spine density, synaptic density measures. and ultrastructural parameters by means, Student t-test, with a $p < 0.05$ considered statistically significant, and Mann-Whitney U test, with a $p < 0.05$ considered statistically significant. For the PVH data, the mean of the glial coverage ratio of all 8 neurons for each animal was taken. The WT and KO means were respectively pooled and Student t-test was performed with a $p < 0.05$ considered statistically significant. OXT immunlabeled neuron glial coverage data was processed in the same way.

Results

qEM of mPFC

Ultrastructural parameters implicating synaptic efficacy were quantified in electron micrographs taken in layer 2/3 of the pre-limbic mPFC. Electron micrographs at 20,000X mag were taken of WT (n = 3) and CNTNAP2 KO mice (n = 3). The area encompassed by these images is 100 μm2 in which the number of dendritic spines were counted, each of which was measured as shown in **Figure 5.** for a set of ultrastructural parameters with a focus on postsynapse. We observed a significant (~25%) reduction in the number of spines profiles with visible PSDs in KO mice (**Fig. 7 B**). The number of these spine profiles with visible presynaptic terminal partners were taken as the measure for asymmetric (putative excitatory) synapse number. Regarding the ultrastructural parameters measured, we found no significant change in spine area or PSD length in KO mice (**Fig. 7 C-D**). We did, however, find that KO mice had a reduced number of multi-synaptic boutons (**Fig. 7 E**). Interestingly, we also found an increase in perforated post-synaptic densities in KO mice (**Fig. 7 F**). A significant decrease in MSB number and a significant increase in pPSD number is seemingly counterintuitive as both MSBs and pPSDs are markers of robust synaptic function. A decrease in presynaptic efficacy concomitant to an increase in postsynaptic function is a perplexing finding. Also, we found a significant decrease in symmetric (putative inhibitory) synapse number (**Fig. 7 G**). Together, these findings indicate that KO mice have significant defects in asymmetric and symmetric (putative E/I) synaptic density as well as alterations in markers of synapse plasticity and stability.

qEM of PVH

The quantitative analysis of glial endfoot coverage in non-IHC labeled material of non-specific magnocellular neurons in the PVH compared the glial coverage ratio of the 3 WT and 3 KO mice. Here, without specific immune labeling, adjacent oxytocinergic and vasopressinergic cells were measured in an unknown proportion (**Figure 8. A**). The glial coverage ratios measured for each of the 8 neurons were averaged giving an animal mean glial coverage ratio; the mean ratios for the 3 WT and 3 KO mice were respectively pooled giving a

mean of means for WT = 0.376 and KO = 0.346. *Students-t* test was preformed yielding no significant difference between glial coverage ratio of WT as compared to KO, see **Figure 9. A** (p = 0.521)

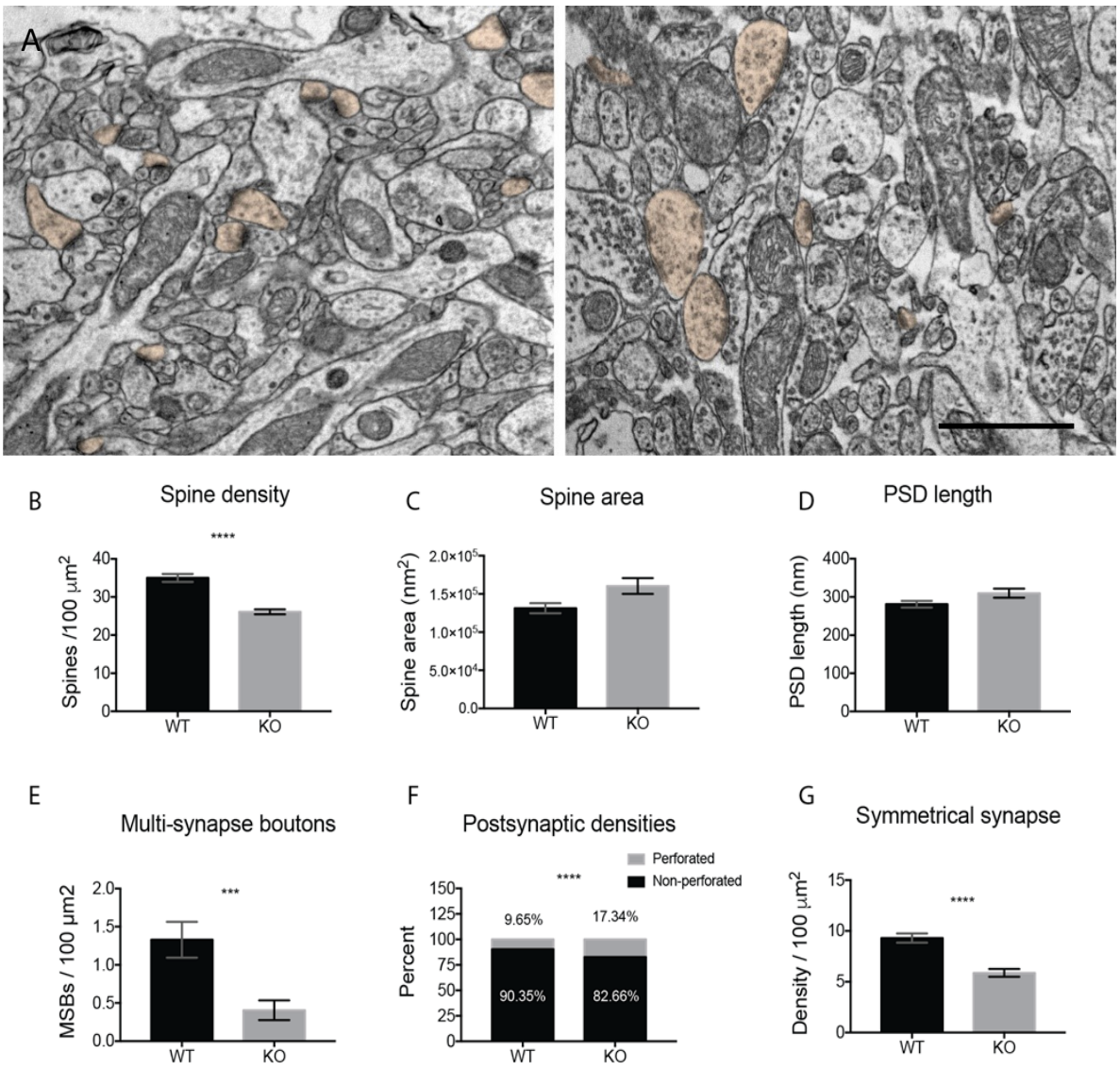

Figure 7. Ultrastructural analysis of the mPFC. A. Electron micrographs of neuropil of L2/3 mPFC in Cntnap2 WT and KO mice (20,000 X mag). Orange pseudo-color is applied to spine profiles. All p values given are from Mann Whitney tests. Scale bar: 500 nm. B-G. Graphs show quantification of synaptic ultrastructure **B.** density of asymmetric (putative excitatory: WT 11.53 ± 0.35 synapses/100 µm2, n = 80 fields; KO 8.59 ± 0.21 synapses/100 µm2, n = 90 fields; 3 mice per genotype; p < 0.0001) and **C.** Spine profile mean area (WT 0.131.30 ± 0.006.58 µm2, n = 257 spines; KO 0.160.40 ± 0.010.26 µm2, n = 187 spines; p = 0.1142) and **D.** PSD length (WT 281.10 ± 8.89 nm, n = 257 spines; KO 309.90 ± 11.83 nm, n = 187 spines; p = 0.0709). **E.** Density of MSBs for WT (1.33 ± 0.23 MSBs per 100 µm2, n = 80 fields) and KO (0.41 ± 0.13 MSBs per 100 µm2, n = 90 fields); p = 0.0002). **F.** Perforated post synaptic densities (pPSDs) for WT (3.38 ± 0.31 pPSD per 100 µm2, n = 90 fields) and KO (4.52 ± 0.31 pPSD per 100 µm2, n = 80 fields); p = 0.0122. G. Symmetric (putative inhibitory: WT 9.30 ± 0.46 synapses/100 µm2, n = 80 fields; KO 5.87 ± 0.38 synapses/100 µm2, n = 90 fields; p < 0.0001) synapses.

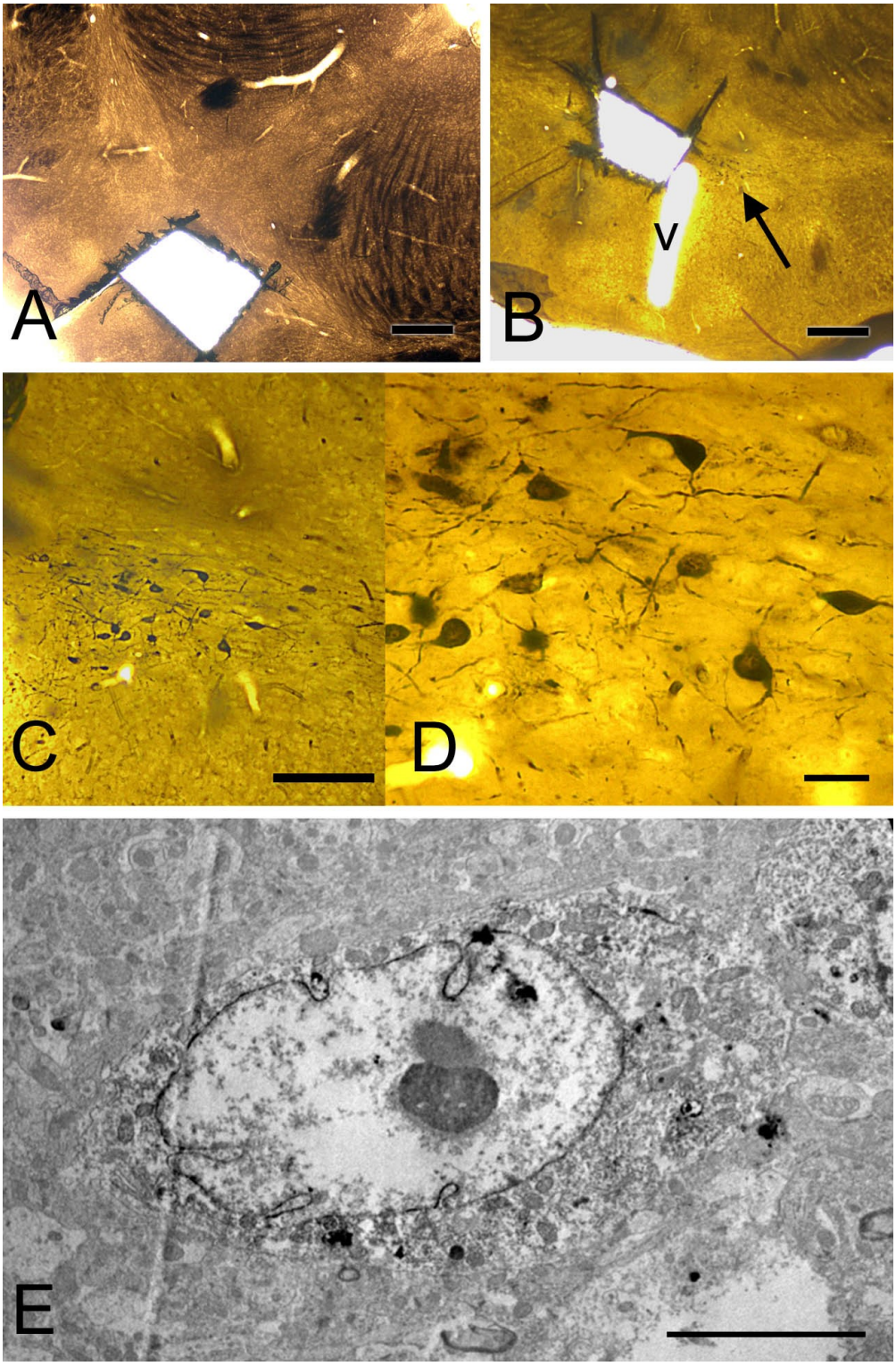

Figure 8. Light and electronmicroscopy of the PVH A. Native resin embedded section with cut-out trapezoid (for ultrathin sectioning), Scale bar: 1mm **B.** Resin embedded section with pre-embedding OXT immune reaction, Scale bar: 1 mm. **C.** PVH magnocellular division with OXT neuron somata and projections visibly marked by IHC, DAB reaction, Scale bar: 50 µm. **D.** Close-up of OXT marked magnocellular neurons, Scale bar 25 µm. **E.** Electron micrograph showing OXT neuron identified by the dark immunoprecipitate within the cytoplasm and by specific immune reactive puncta of DAB. 6000X mag, Scale bar: 5 µm

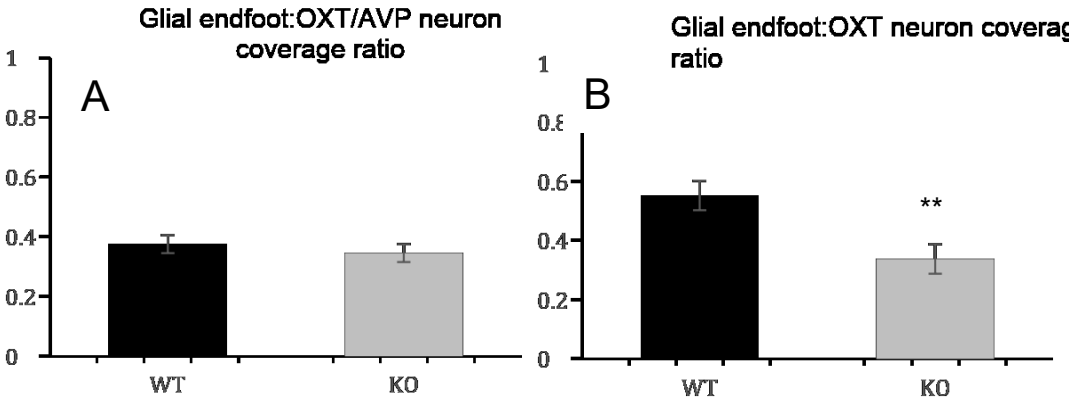

Figure 9. Ultrastructural analysis of the glial coverage of non-identified and IHC identified magnocellular neurons in the PVH. A. WT SE = 0.035, KO SE = 0.031 **B.** Glial endfoot:OXT neuron coverage, WT SE = 0.064, KO SE = 0.056. **= $p < 0.05$

Glial coverage ratio of immune-labeled oxytocinergic magnocellular neurons of the PVH were compared between a single WT and a KO animal. The glial coverage ratio of the WT animal had a mean = 0.552, the KO animal had a mean ratio = 0.337, see **Figure 9. B**. Students t-test was performed showing a significant difference between the KO and the WT means of the animals ($p < 0.05$). Thus, in our single mouse comparison, glial coverage of OXT magnocellular neurons was found to be significantly less in KO as compared to WT ($p = 0.024$), encouraging further investigations.

Discussion

mPFC findings in context

In both brain regions, mPFC and PVH, our qEM findings suggest mechanistic differences between CNTNAP2 KO and WT. In layer 2/3 of the prelimbic mPFC our findings of decreased asymmetrical synapse number (putative excitatory synapse density) and decreased symmetrical synapse number (putative inhibitory synapse density) corroborate the network E/I imbalance findings of Lazaro 2017. Anatomical differences in dendrite morphology and spine density at light microscopic mag. were found by our collaborators; particularly: decreased spine density in pyramidal neurons was found (Lazaro, 2017). Our structural qEM data of decreased inhibitory and excitatory synapse number supports the reported decrease in functional excitatory and inhibitory synaptic inputs measured in L2/3 mPFC with delayed phase-firing and reduced phase-locking of inhibitory and excitatory neurons.

Recent innovative studies demonstrate a direct link between social behavioral abnormality and mPFC network activity. Behavioral abnormalities were rescued in CNTNAP2 KO mice by modulation of E/I imbalance in a study by Selimbeyogulu et al. 2017. With the use of a stabilized step-function opsin (SSFO) tool, optogenetically increasing the excitability of inhibitory parvalbumin neurons or decreasing the excitability of excitatory pyramidal neurons allowed for real-time modulation of neuronal circuits during social behavior (Selimbeyogulu et al., 2017). Hyperactivity in open-field test, and significantly decreased time of interaction and exploration in social interaction test were rescued by SSFO activation of parvalbumin neurons (Selimbeyogulu et al., 2017). These findings bring our data of E/I imbalance to life with a direct link to social behavioral abnormality. Additionally, Lazaro 2017 links E/I imbalance to social interaction in a novel headfixed social interaction test combined with live silicon microprobe patchclamp recording. Either a mouse or an empty cup containing cage was remotely rotated in front of a headfixed mouse within whisker touching distance concurrent to live cell activity recording. CNTNAP2 KO mice interacted with significantly less preference for the caged mouse versus the cup compared to WT mice. Paired with live cell recordings, these findings show a significant difference in mPFC network functionality linked to impaired social interaction.

Our findings of a significant increase in the number of pPSDs concurrent with a significant decrease of MSBs in KO animals compared to WT animals are mechanistically

intriguing. Both pPSDs and MSBs reflect robust synaptic function (Sorra and Harris, 1993; Bourne and Harris, 2008). Our findings are indicative of neuropil with powerful postsynaptic efficacy concurrent to a less robust presynapse. With the knowledge of CNTNAP2 expression both pre and postsynaptically, as well as its multifaceted structural and functional roles as a neurexin, it is tantalizing to speculate a transsynaptic mechanistic difference in CDFE (Sudhof et al., 2008; Poot et al., 2015).

PVH findings in context

In the PVH our findings hint at structural change in the central oxytocin system. OXT is hotly explored with human clinical trials of intranasal application yielding promising results in alleviating social challenges/debilitations (Mitre et al., 2018). The combination of intranasal OXT and task-based fMRI links the activation of brain areas implicated in social-emotional processing to OXT stimuli (Zhao et al., 2017). More specifically, intranasal OXT has been found to decrease amygdala activation resulting in increased observable 'trust', increased duration of direct eye contact and an improvement of recognition of social cues (McGregor et al., 2008). These findings link various brain regions with complex social functionality to levels of OXT. OXT levels are effectively lower in people with ASD; increasing OXT level in autistic brain has profound social effect. In observing the PVH, the structural basis of the natural production of OXT is investigated. As such, our preliminary findings of variable glial coverage of OXT magnocellular perikarya are set within the brain-wide effects of OXT on social behavior in ASD.

Unpublished data from Illana Gozes indicate that OXT intranasal application has a dramatic short-term effect on sociability of people with ASD; recent human clinical trials show almost immediate and significant improvement of facial emotional recognition with intranasal OXT application (Gozes, 2017). OXT intranasally acts directly through the bloodstream; alleviating social difficulties of people with ASD has the potential of alleviating much suffering (Parker et al. 2017).

These findings indicate a notable difference in function of the central oxytocin system. Central to this action is the function of the PVH which is in close proximity to both CSF (straddling the 3rd ventricle) and blood (close contact with capillaries running through the hypothalamus). The mechanism of transmission of OXT within the brain is classically understood similar to that of dopamine, OXT diffuses from projections of the supraoptic and

paraventricular hypothalamic nucleus to brain regions implicated in social behavior and processing (Argiolas and Gessa, 1990). Recently, the synaptic presence of OXT receptors has been demonstrated (Bakos et al., 2018). Our qEM results of native PVH did not distinguish between adjacent oxytocinergic and vasopressinergic cells. The proportion of which neurons were measured in native contrast is unknown. Thereby we aimed to measure general glial coverage of the region with no significant difference found.

In immune labeling OXT neurons of the magnocellular division of the PVH we looked to narrow our precision of measurement of glial coverage specifically to exclude the vasopressin system. As the first round of our study, we specifically labeled OXT neurons of 1 KO and 1 WT mouse. Our findings of significant decreased glial coverage of OXT neurons of a KO animal compared to a WT animal ($p = 0.024$) point towards a potential mechanism of central regulatory OXT function which may be structurally observed. With these findings, the trend of the native contrast data: slightly lower KO glial coverage ratio as compared to WT may be marginally noted.

Mechanistically two considerations come to mind with this increased area of neuronal somatic membrane exposure. Firstly, there is increased area for E/I terminal influence on OXT perikarya. Secondly, the electrochemical balance of the milieu surrounding the neuron may very well influence OXT neuron functionality as glial endfoot coverage regulates the extracellular milieu around neurons (Dityatev et al., 2006). From our initial findings we hypothesize a change of the electrochemical environmental balance of OXT magnocellular neurons of the PVH in our CNTNAP2 KO model which may be tied to decreased glial endfoot coverage of the neurons' somata. We look to test this hypothesis by extending our sample size to the full 3 WT and 3 KO animals at our disposal with the same pre-embedding OXT IHC and qEM. CNTNAP2 function fits well into this mechanistic frame work as it is implicated in neuronal-glia interaction (Gdalyahu et al., 2015).

Conclusion

We used qEM in two distinct brain regions directly linked to social behavior in integrative (mPFC) and manifest (PVH) ways to chip away at the neurobiological mechanisms underlying CDFE. Linking structural quantitative data to the nebulous complex question of how the autistic brain functions may be a remarkably useful approach for the neuroscience community in exploring autism in the future.

Acknowledgements

The following grants made this work available:

a) „This Project is supported by the European Union and co-financed by the European Social Fund (grant agreement no. EFOP-3.6.2-16-2017-00008, project title: *The role of neuro-inflammation in neurodegeneration: form molecules to clinics*)"

b) The János Bolyai research Fellowship of the Hungarian Academy of Sciences and the ÚNKP Bolyai+ grant of the Ministry of Human Capacities to my Supervisor, Bence Rácz

I would like to thank my supervisor Rácz Bence for his enduring support, mentorship, and humor making our work light and enjoyable. I would like to thank our EM lab technician Tünde Magyar for her practical lessons, and her help processing samples from intact brains to grids; I would like to extend a special thanks to her for the ultrasectioning. I would like to extend my thanks to Renáta Pop for all her help in operating and centering the electron microscope. I would like to thank our collaborators: Maria Lazaro and Katrina Choe for their good work in the mPFC and the PVN respectively; an additional thanks to them for help with the conceptual design of our experiments. I would like to extend a special thanks to my mom and family for their support and patience. Lastly, I would like to thank my wonderful girlfriend, Chanett, for her sublime support and kindness through the entire course of this project, and our dogs Phil and Laura for their support and patience with some shorter walks.

Abstract

In unraveling the complex cognitive differences of autism spectrum disorders (ASD) the structure-function relationship based analysis of quantitative electron microscopy (qEM) is a notable asset to a range of studies. Morphology remarkably reflects mechanisms in the brain. As such, qEM fits well with electrophysiological and projection mapping studies. Here, we studied a loss of function mutation in contactin associated protein-like 2 (CNTNAP2) causing a syndromic form of autism spectrum disorder in humans; CNTNAP2 KO in mice produces social deficits, repetitive behaviors, and seizures. We investigated synaptic ultrastructural differences between CNTNAP2 KO and WT with qEM in the pre-limbic area of the mouse medial pre-frontal cortex (mPFC), and we also analyzed glial coverage in the magnocellular division of the mouse paraventricular hypothalamic nucleus (PVH) in the context of the oxytocin system within the brain. Our results show, that the loss of the CNTNAP2 gene may play a crucial role in the development of the structural basis of ASD.

Összefoglaló

Autizmus spektrum rendellenességek (autism spectrum disorders [ASD]) sokrétű és komplex kognitív elváltozásainak feltárásában több kutatás jelentős segítségére válik a kvantitatív elektronmikroszkópia (quantitative electron microscopy [qEM]) szerkezet-funkció alapú megközelítése. Az idegszövetben a morfológia hűen tükrözi a hálózat funkcionális változásait. Így a qEM értékes adatokkal szolgálhat a funkcionális kutatásokhoz. Egy nagyobb elektrofiziológiai és viselkedési kísérlet részeként az ASD sok megnyilvánulásából egy funkcióvesztett contactin associated protein-like 2 (CNTNAP2 KO) mutációt tanulmányoztunk egér modellen. Egérben is megfigyelhető, hogy a CNTNAP2 hiány szociális hiányosságokhoz, repetitív viselkedéshez, és epilepsziás rohamokhoz vezet. qEM-el szinaptikus ultrastrukturális elváltozásokat vizsgáltunk KO és WT egyedek között a pre-limbikus mediális pre-frontális kéregben, valamint az autizmusban szintén érintett paraventrikuláris hypotalamikus mag (paraventricular hypothalamic nucleus [PVH]) oxitocin-tartalmú sejtjeinek glia-kapcsolatait is feltártuk. Eredményeink szerint a CNTANP2 gén hiánya számos, as ASD-ben megfigyelhető szerkezeti változásért tehető felelőssé.

References

Image on cover: photo of original painting by G. Mark Marcello

Anderson, G. R., Gal, T., Xu, W., Aoto, J., Malenka, R. C., & Südhof, T. C. (2012). Candidate autism gene screen identi fi es critical role for cell-adhesion molecule CASPR2 in dendritic arborization and spine development. https://doi.org/10.1073/pnas.1216398109/-/DCSupplemental.www.pnas.org/cgi/doi/10.1073/pnas.1216398109

Argiolas, A., & Gessa, G. L. (1991). Central functions of oxytocin. *Neuroscience and Biobehavioral Reviews*, *15*(2), 217–231. https://doi.org/10.1016/S0149-7634(05)80002-8

Autism Spectrum Disorder (ASD). (2018, April 26). Retrieved from https://www.cdc.gov/ncbddd/autism/data.html

B6.129(Cg)-Cntnap2tm1Pele/J. (2018). Retrieved from https://www.jax.org/strain/017482

Bakos, J., Srancikova, A., Havranek, T., & Bacova, Z. (2018). Molecular Mechanisms of Oxytocin Signaling at the Synaptic Connection. *Neural Plasticity*, *2018*, 1–9. https://doi.org/10.1155/2018/4864107

Ben-Barak, Y., Russell, J. T., Whitnall, M. H., Ozato, K., & Gainer, H. (1985). Neurophysin in the hypothalamo-neurohypophysial system. I. Production and characterization of monoclonal antibodies. *The Journal of Neuroscience : The Official Journal of the Society for Neuroscience*, *5*(1), 81–97. Retrieved from http://www.ncbi.nlm.nih.gov/pubmed/3880813

Bourne, J. N., & Harris, K. M. (2008). Balancing Structure and Function at Hippocampal Dendritic Spines. Annu Rev Neurosci, 31, 47–67. https://doi.org/10.1146/annurev.neuro.31.060407.125646.

Brophy, P. J. (2003). Myelinated Nerves: Filling in the Juxtaparanodal Gap. *Current Biology*, *13*(24), R956–R957. https://doi.org/10.1016/j.cub.2003.11.041

de Wied, D., Diamant, M., & Fodor, M. (1993). Central nervous system effects of the neurohypophyseal hormones and related peptides. Frontiers in Neuroendocrinology. https://doi.org/10.1006/frne.1993.1009

Dityatev, A., Frischnecht, R., Seidenbecher, C., (2006). Extracellular matrix and synaptic functions. *Results and Problems in Cell Differentiation, 43,* 69-97.

Foxe, J. J., Molholm, S., Baudouin, S. J., & Wallace, M. T. (2018). Explorations and perspectives on the neurobiological bases of autism spectrum disorder. *European Journal of Neuroscience*, *47*(6), 488–496. https://doi.org/10.1111/ejn.13902

Gdalyahu, A., Lazaro, M., Penagarikano, O., & Golshani, P. (2015). The Autism Related Protein Contactin- Stabilizes New Spines : An In Vivo Mouse Study, *2*, 1–7. https://doi.org/10.1371/journal.pone.0125633

Gozes, I. (2017). *Translational neuroscience: from the lab bench to clinical trials.* FENS Regional Meeting, Pécs, 20-23 September 2017.

Grandin, T., (2010). *The world needs all kinds of minds.* Retrieved from https://www.ted.com/talks/temple_grandin_the_world_needs_all_kinds_of_minds/up-next?referrer=playlist-the_autism_spectrum

Harris, K. M. (1999). Structure, development, and plasticity of dendritic spines. Current Opinion in Neurobiology, 9(3), 343–348. https://doi.org/10.1016/S0959-4388(99)80050-6

Harris, K. M., & Weinberg, R. (2012). Mammalian Brain. *Cold Spring Harbor Perspectives in Biology*, *4*, 1–30.

Kniffin, C. L. (2017, September 07). CONTACTIN-ASSOCIATED PROTEIN-LIKE 2; CNTNAP2. Retrieved from https://www.omim.org/entry/604569

Lazaro, M.T. (2017). *Synaptic and network abnormalities in the medial prefrontal cortex of the CNTNAP2 mouse model of autism.* UCLA Electronic Theses and Dissertations.

Lazaro, M. T., Taxidis, J., Shuman, T., Bachmutsky, I., Ikrar, T., Santos, R., Marcello, G. M., Mylavarapu, A., Chandra, S., Foreman, A., Goli, R., Sharma, N., Tran, D., Azhdam, M., Dong, H., Peñagarikano, O., Masmanidis, S., Rácz, B., Xu, X., Geschwind, D., Golshani, P. (2018). Reduced prefrontal synaptic connectivity and disturbed oscillatory population dynamics in the CNTNAP2 model of autism. *BioRxiv*. Retrieved from http://biorxiv.org/content/early/2018/05/15/322388.1.abstract.

Marcello, G., Szabó, L., Sotonyi, P., & Rácz, B. (2018). Quantitative Electron Microscopic Assay Using Random Sampling from Single Sections to Test Plastic Synaptic Changes in Hippocampus. *Bio-Protocol*, *8*(15), 1–10. https://doi.org/10.21769/BioProtoc.2946

Mitre, M., Minder, J., Morina, E. X., Chao, M. V., & Froemke, R. C. (2018). Oxytocin Modulation of Neural Circuits. *Curr Top Behav Neuroscience*, (July 2018), 31–53. https://doi.org/10.1007/7854

Parker, K. J., Oztan, O., Libove, R. A., Sumiyoshi, R. D., Jackson, L. P., Karhson, D. S., … Hardan, A. Y. (2017). Intranasal oxytocin treatment for social deficits and biomarkers of response in children with autism. Proceedings of the National Academy of Sciences, 114(30), 201705521. https://doi.org/10.1073/pnas.1705521114

Peñagarikano, O., Abrahams, B. S., Herman, E. I., Winden, K. D., Gdalyahu, A., Dong, H., … Geschwind, D. H. (2011). Absence of CNTNAP2 leads to epilepsy, neuronal migration abnormalities, and core autism-related deficits. *Cell*, *147*(1), 235–246. https://doi.org/10.1016/j.cell.2011.08.040

Peñagarikano, O., Lázaro, M. T., Lu, X.-H., Gordon, A., Dong, H., Lam, H. A., … Geschwind, D. H. (2015). Exogenous and evoked oxytocin restores social behavior in the *Cntnap2* mouse model of autism. *Science Translational Medicine*, *7*(271), 271ra8-271ra8. https://doi.org/10.1126/scitranslmed.3010257

Poliak, S., Gollan, L., Martinez, R., Custer, A., Einheber, S., Salzer, J. L., … Peles, E. (1999). Caspr2, a new member of the Neurexin superfamily, is localized at the juxtaparanodes

of myelinated axons and associates with K+channels. *Neuron*, *24*(4), 1037–1047. https://doi.org/10.1016/S0896-6273(00)81049-1

Poliak, S., Salomon, D., Elhanany, H., Sabanay, H., Kiernan, B., Pevny, L., … Peles, E. (2003). Juxtaparanodal clustering of Shaker-like K+channels in myelinated axons depends on Caspr2 and TAG-1. *Journal of Cell Biology*, *162*(6), 1149–1160. https://doi.org/10.1083/jcb.200305018

Poot, M. (2015). Connecting the CNTNAP2 networks with neurodevelopmental disorders. *Molecular Syndromology*, *6*(1), 7–22. https://doi.org/10.1159/000371594

Racz, B., & Weinberg, R. J. (2006). Spatial organization of cofilin in dendritic spines. *Neuroscience*, *138*(2), 447–456. https://doi.org/10.1016/j.neuroscience.2005.11.025

Rodenas-Cuadrado, P., Ho, J., & Vernes, S. C. (2014). Shining a light on CNTNAP2: Complex functions to complex disorders. *European Journal of Human Genetics*, *22*(2), 171–178. https://doi.org/10.1038/ejhg.2013.100

Selimbeyoglu, A., Kim, C. K., Inoue, M., Lee, S. Y., Hong, A. S. O., Kauvar, I., … Deisseroth, K. (2017). Modulation of prefrontal cortex excitation / inhibition balance rescues social behavior in CNTNAP2 -deficient mice. *Science Translational Medicine*, *9*(401), eaah6733. https://doi.org/10.1126/scitranslmed.aah6733

Südhof, T. C. (2008). Neuroligins and neurexins link synaptic function to cognitive disease. *Nature*, *455*(7215), 903–911. https://doi.org/10.1038/nature07456

Theodosis, D. T., Chapman, D. B., Montagnese, C., Poulain, D. A., & Morris, J. F. (1986). Structural plasticity in the hypothalamic supraoptic nucleus at lactation affects oxytocin-, but not vasopressin-secreting neurones. *Neuroscience*, *17*(3). https://doi.org/10.1016/0306-4522(86)90038-2

Weiss, J. A., Baker, J. K., & Butter, E. M. (2016, September). Mental health treatment for people with autism spectrum disorder (ASD). Retrieved from https://www.apa.org/pi/disability/resources/publications/newsletter/2016/09/autism-spectrum-disorder.aspx